Near-field correlations in down-converted light with a strongly focused pump

F.M.G.J. Coppens

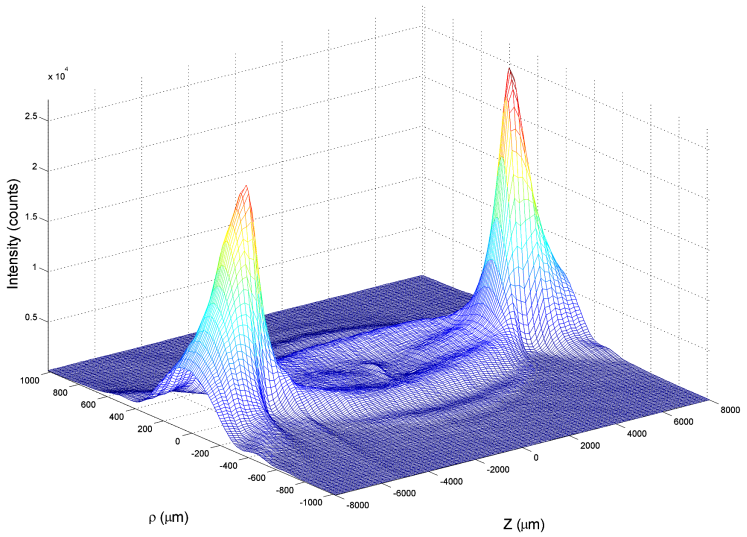

Quantum Optics and Quantum Information group
November 24, 2010
This project was supervised by:
Drs. H. Di Lorenzo Pires
Dr. M.P. van Exter

Contents

1 Introduction

In this report we will study the near-field correlations in the two-photon field generated by a non-linear process called *spontaneous parametric down conversion*, or SPDC for short. The research done in this report builds on previous research[1, 2] conducted by H. Di Lorenzo Pires and M. P. van Exter. They studied the near-field correlations in down-converted light generated by pumping a thin periodically poled potassium titanyl phosphate ($KTiOPO_4$) crystal (PPKTP) with a collimated continuous wave laser. By collimated we mean that the depth of the focus (twice the Rayleigh range) is much longer than the thickness of the crystal. They have shown that the spatial structure of this two-photon field can be described by a correlation function of form $A(\boldsymbol{\rho}_s, \boldsymbol{\rho}_s; Z_d) \propto V\left(\frac{\boldsymbol{\rho}_s - \boldsymbol{\rho}_i}{2}; Z_d\right)$, where $\boldsymbol{\rho}_s$ and $\boldsymbol{\rho}_i$ are the transverse coordinates of the generated *signal* and *idler* photon pair and Z_d is the imaged z-plane of the detection modes. This correlation function gives the *probability amplitude* of a joint detection by two single photon counters. The squared amplitude tells us what the probability is of finding the idler photon at location $\boldsymbol{\rho}_i$ provided that the signal photon is at location $\boldsymbol{\rho}_s$.

In this research we study the case where the focus depth is much shorter than the thickness of the crystal. In this case we show that the correlation function is modified and can be written like $A(\boldsymbol{\rho}_s, \boldsymbol{\rho}_s; Z_p, Z_d) \propto G\left(\frac{\boldsymbol{\rho}_s + \boldsymbol{\rho}_i}{2}; Z_p - Z_d\right) \times V\left(\frac{\boldsymbol{\rho}_s - \boldsymbol{\rho}_i}{2}; Z_d\right)$, where an extra factor 'G' appears. This factor depends on the sum coordinates and on the separation distance between the pump focus and the detection modes. This is a Gaussian beam profile depending on the focussing details of the pump. Because the crystal is so big there is an extra degree of freedom in which we can now scan the detection modes with respect to the focus of the pump. The most striking feature of the considered strong focussing regime is the fact that by focussing the pump we can map the structure of the two-photon correlations into a single-photon intensity field. We will show that the structures in this field are equal in size to that of the two-photon field.

2 Theory

2.1 Two-photon field

We consider the geometry depicted in Fig. 1 on page 11 for a frequency degenerate ($k_p = 2k_d$) situation. In the case where a collimated pump ($z_p \gg L$) is used the probability amplitude of the projected two-photon field onto the detection modes is given by[3, 1]:

$$A_{proj}(\boldsymbol{\rho}_s, \boldsymbol{\rho}_i; Z_d) \propto \int_{-L/2-Z_d}^{+L/2-Z_d} dz \; \frac{e^{i\Delta k_z^0 z}}{z + iz_d} \times \exp\left[\frac{-ik_d|\boldsymbol{\rho}_-|^2}{z + iz_d}\right], \tag{1}$$

where Z_d is defined as the displacement from $z = 0$, the center of the crystal, z_d is the Rayleigh range of the detection modes, Δk_z^0 is the on-axis phase mismatch in vacuum (when the signal and idler photons travel parallel to the beam axis). Furthermore, $\boldsymbol{\rho}_\pm \equiv \frac{\boldsymbol{\rho}_s \pm \boldsymbol{\rho}_i}{2}$, such that $\boldsymbol{\rho}_s = \boldsymbol{\rho}_+ + \boldsymbol{\rho}_-$ and $\boldsymbol{\rho}_i = \boldsymbol{\rho}_+ - \boldsymbol{\rho}_-$. This formula is most often referred to as the *two-photon correlation function*. It tells you what the probability is of measuring an idler photon with a detector positioned at $\boldsymbol{\rho}_i$ provided that the signal photon is observed with a detector positioned at $\boldsymbol{\rho}_s$.

In the case where we strongly focus the pump ($z_p \ll L$) we have to take the shape of the pump into account. The resulting two-photon correlation function becomes slightly different. In order to calculate it, we set up a cylindrical coordinate system where the beam is propagating in the $\hat{z}$-direction and $\boldsymbol{\rho}_j$, $j \in \{s, i\}$, is the transverse coordinate for the signal and idler detection modes respectively. Since the Rayleigh range of the pump and detection modes is stretched due to the higher refractive index of the crystal we must compensate for this. The waist of the modes are unaffected. We define the Rayleigh range as $z_l = \frac{1}{2} n_l k_l^0 w_l^2$, $l \in \{p, d\}$, where n_l is the refractive index in the crystal at the generated wavelength, k_l^0 is the wave number in vacuum and $k_l = n_l k_l^0$. Also the displacement of the pump and detection modes are stretched, so we define $Z_l = n_l Z_l^0$, where Z_l^0 is the displacement from $z = 0$ in vacuum. The projection of two-photon field onto the detection modes is then given by the following integral[1]:

$$\begin{aligned} A_{proj}(\boldsymbol{\rho}_s, \boldsymbol{\rho}_s; Z_p, Z_d) \propto \int_{-L/2}^{+L/2} dz \int_{-\infty}^{+\infty} d\boldsymbol{\rho} \; E_p(\boldsymbol{\rho}; z - Z_p) \\ \times \phi_s^*(\boldsymbol{\rho} - \boldsymbol{\rho}_s; z - Z_d)\phi_i^*(\boldsymbol{\rho} - \boldsymbol{\rho}_i; z - Z_d), \end{aligned} \tag{2}$$

where the first integration is done over the crystal length L and the second integration over the transverse dimension of the crystal. Because the transverse dimension of the crystal is much larger than the waist of the pump we have set the boundaries at infinity.

E_p and ϕ_d^* are the Gaussian mode profiles of the pump and detection modes:

$$E_p(\boldsymbol{\rho}; z) \propto \frac{e^{ik_p z}}{z - iz_p} \exp\left[\frac{ik_p|\boldsymbol{\rho}|^2}{2(z - iz_p)}\right], \tag{3}$$

$$\phi_d^*(\boldsymbol{\rho}; z) \propto \frac{e^{-ik_d z}}{z + iz_d} \exp\left[\frac{-ik_d|\boldsymbol{\rho}|^2}{2(z + iz_d)}\right]. \tag{4}$$

After substituting Eqs. (3) and (4) into Eq. (2) the integrals becomes:

$$A_{proj}(\boldsymbol{\rho}_s, \boldsymbol{\rho}_s; Z_p, Z_d) \propto \frac{\exp\left[-\frac{k_d|\boldsymbol{\rho}_+|^2}{z_d+z_p+i(Z_d-Z_p)}\right]}{z_d+z_p+i(Z_d-Z_p)} \times \int_{-L/2-Z_d}^{+L/2-Z_d} dz\ \frac{e^{i\Delta k_z^0 z}}{z+iz_d} \times \exp\left[\frac{-ik_d|\boldsymbol{\rho}_-|^2}{z+iz_d}\right]. \quad (5)$$

Notice that the part inside the integral is the same as for the collimated case, the only difference is the factor in front of the integral.

The projected two-photon probability amplitude can thus be written like

$$A_{proj}(\boldsymbol{\rho}_s, \boldsymbol{\rho}_s; Z_p, Z_d) \propto G(\boldsymbol{\rho}_+; Z_p - Z_d) \times V(\boldsymbol{\rho}_-; Z_d), \quad (6)$$

where $G(\boldsymbol{\rho}_+; Z_p - Z_d)$ is a Gaussian beam profile depending primarily on the sum coordinate $\boldsymbol{\rho}_+$ and on the focussing of the pump. All details about the near-field correlations are contained in $V(\boldsymbol{\rho}_-; Z_d)$.

The coincidence count rate R_{cc} assumes the form:

$$R_{cc}(\boldsymbol{\rho}_s, \boldsymbol{\rho}_s; Z_p, Z_d) \propto \frac{\exp\left[-\frac{2k_d(z_d+z_p)|\boldsymbol{\rho}_+|^2}{(z_d+z_p)^2+(Z_d-Z_p)^2}\right]}{(z_d+z_p)^2+(Z_d-Z_p)^2} \times \left| \int_{-L/2-Z_d}^{+L/2-Z_d} dz\ \frac{e^{i\Delta k_z^0 z}}{z+iz_d} \times \exp\left[\frac{-ik_d|\boldsymbol{\rho}_-|^2}{z+iz_d}\right] \right|^2. \quad (7)$$

2.2 One-photon field

2.2.1 Near-field profile

Once the correlation function of the two-photon field is known it is straightforward to calculate the single-photon intensity. The intensity of the single-photon field is calculated by taking the partial trace of the two-photon correlation function. This is equivalent to integrating over all possible positions of one of the two photons, effectively summing the joint probabilities of photon one being at some fixed position and photon two being at *any other* position. Just like adding the rows together of a square matrix and leaving a vector. This leaves the probability amplitude as a function of only the position of one photon. The intensity is thus given by:

$$I(\boldsymbol{\rho}; Z_p, Z_d) = \int d\boldsymbol{\rho}'\ \left|A_{proj}(\boldsymbol{\rho}', \boldsymbol{\rho}; Z_p, Z_d)\right|^2 \quad (8)$$

$$= \int d\boldsymbol{\rho}'\ A^*_{proj}(\boldsymbol{\rho}', \boldsymbol{\rho}; Z_p, Z_d)\ A_{proj}(\boldsymbol{\rho}, \boldsymbol{\rho}'; Z_p, Z_d) \quad (9)$$

$$= \int d\boldsymbol{\rho}'\ \left|G\left(\frac{\boldsymbol{\rho}'+\boldsymbol{\rho}}{2}; Z_p - Z_d\right)\right|^2\ \left|V\left(\frac{\boldsymbol{\rho}'-\boldsymbol{\rho}}{2}; Z_d\right)\right|^2 \quad (10)$$

Because the pump is very strongly focused and its spatial extend is much smaller than that of the transverse SPDC structure, which is about 100μm as opposed

to the 22 μm of the pump, we may approximate G with a Dirac-delta function. The intensity now becomes

$$I(\boldsymbol{\rho}; Z_d) \approx \int d\boldsymbol{\rho}' \left|\delta\left(\frac{\boldsymbol{\rho}' + \boldsymbol{\rho}}{2}\right)\right|^2 \left|V\left(\frac{\boldsymbol{\rho}' - \boldsymbol{\rho}}{2}; Z_d\right)\right|^2 \tag{11}$$

$$= \left|V(\boldsymbol{\rho}; Z_d)\right|^2 \tag{12}$$

So, strongly focussing the pump acts as a mechanism for mapping the correlations in the two-photon field to an intensity profile in the one-photon field.

2.2.2 Far-field profile

To fit the far-field measurements in Section 3.2.1 we need to calculate the angular one-photon intensity profile. The momentum representation of the two-photon field is[4, 5]:

$$\tilde{A}(\boldsymbol{q}_s, \boldsymbol{q}_s) = \tilde{E}(\boldsymbol{q}_s + \boldsymbol{q}_i)\ \mathrm{sinc}\left(\frac{1}{2}\Delta k_z L\right), \tag{13}$$

where $E(\boldsymbol{q})$ is the angular spectrum of the pump and $\mathrm{sinc}\left(\frac{1}{2}\Delta k_z L\right)$ is the phase-matching function with crystal thickness L and longitudinal wave vector mismatch $\Delta k_z \equiv k_{p,z} - k_{s,z} - k_{i,z}$.

In our geometry $\frac{1}{2}\Delta k_z L$ can be approximated by

$$\frac{1}{2}\Delta k_z L \approx \frac{L}{8nk_0}|\boldsymbol{q}_s - \boldsymbol{q}_i|^2 + \varphi(T), \tag{14}$$

where n is the refractive index at the generated frequency, $k_0 = 2\pi/\lambda_0$ is the vacuum wave vector of the generated light. φ is called the collinear phase mismatch and is an adjustable parameter that depends on the crystal temperature T as[6] $\varphi(T) = \alpha(T - T_0)$.

For a collimated pump the intensity profile of the one-photon angular spectrum is again obtained by taking the partial trace over one of the transverse momenta which leads to the following integral:

$$|\tilde{A}(\boldsymbol{q})|^2 = \int d\boldsymbol{q}'\ \left|\tilde{E}(\boldsymbol{q} + \boldsymbol{q}')\right|^2\ \mathrm{sinc}^2\left(\frac{L}{8nk_0}|\boldsymbol{q} - \boldsymbol{q}'|^2 + \varphi(T)\right) \tag{15}$$

$$\approx \int d\boldsymbol{q}'\ \delta(\boldsymbol{q} + \boldsymbol{q}')\ \mathrm{sinc}^2\left(\frac{L}{8nk_0}|\boldsymbol{q} - \boldsymbol{q}'|^2 + \varphi(T)\right) \tag{16}$$

$$= \mathrm{sinc}^2\left(\frac{L}{2nk_0}|\boldsymbol{q}|^2 + \varphi(T)\right), \tag{17}$$

where we used that a collimated pump has a sharply defined wave vector so it can by approximated by a delta-function.

3 Imaging the one-photon field

3.1 Experimental setup

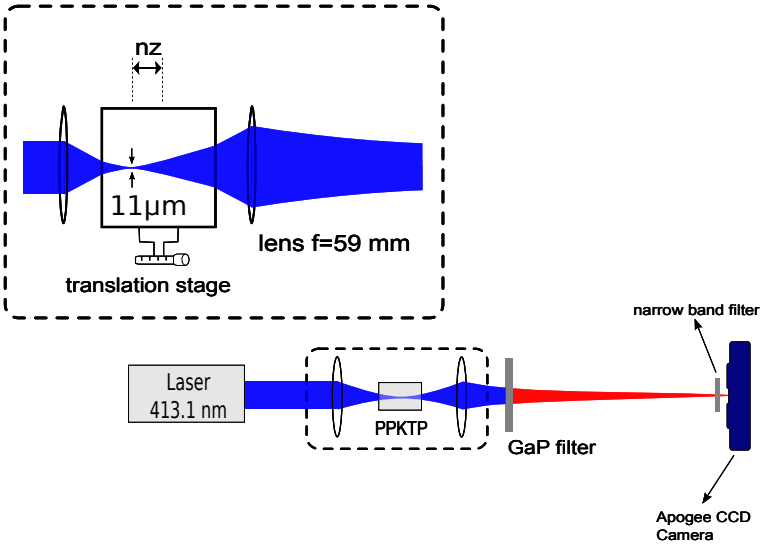

Fig. 1: The experimental setup for imaging the near-field of the one-photon field. The pump laser is strongly focused inside the crystal. We are imaging the vicinity around a plane that coincidences with the focus of the pump. The second lens makes a 10× magnified image of this plane onto a CCD camera. The imaged wavelength is selected by a 5 nm narrow spectral filter centred around λ_0=826 nm, which is twice the wavelength of the pump.

The setup we used is straightforward (see Fig. 1). A 20 mm long periodically-poled KTP (PPKTP for short) crystal is pumped with a Coherent Innova 300 Series cw Krypton-ion laser at λ_0=413.1 nm in a linearly polarized TEM_{00}-mode. Laser power is set to ≈50 mW unless stated otherwise. The beam is reflected by a series of coated mirrors for easy beam placement and targeting. The first active component is a $\lambda/2$-plate, which is used to adjust the polarization of the beam. The beam then travels through a f=100 mm coated lens to be focused inside a 1x2x20 mm PPKTP crystal. The measured spot size is w_0 ≈11 μm. With a Rayleigh range of z_p ≈0.92 mm (in air), this is well within the boundaries of the regime to be studied. The lens is mounted on a manual translation stage with micrometer precision in three orthogonal directions to align the beam waist to coincide with the image plane of the CCD-camera and to make sure that the beam hits the crystal perpendicular to the input facet. The crystal itself is mounted on top of a bulky aluminium structure which is thermally connected to Peltier element to control and stabilize the temperature of the crystal. The Peltier-element is connected to a temperature control and stabilization unit with 10 mK accuracy. This structure is mounted on a translation stage which also has three degrees of freedom in orthogonal directions. It can be adjusted manually in two transverse directions (x, y) with micrometer precision. The longitudinal direction (z) translation is controlled by a Newport

actuator with sub-micrometer precision. The actuator is connected to a Newport ESP 300 motion controller. Behind the crystal, the beam waist is imaged $\approx$10$\times$ magnified on an Apogee Alta U1 CCD-camera by a f=59 mm lens. The size of the CCD-chip is 512$\times$768 pixels with a physical pixel size of 9$\times$9 μm and it has a 16 bit dynamic range. After the second lens we placed a coated GaP-filter to select only the light produced by the SPDC process. No light from the pump laser gets through. Just in front of the camera we placed a λ_0=826 nm band-pass filter with a $\Delta\lambda$=5 nm bandwidth to work in a frequency degenerate regime.

3.1.1 Aligning the pump polarization

To align the polarization of the pump with the optical axis of the crystal one can use the birefringence of the crystal and look at the interference pattern of the pump behind a Glan-Thompson polarizer set perpendicular to the pump polarization. If the pump polarization is not perfectly aligned to the crystal axis interference fringes will appear behind the polarizer (see Fig. 2) due to the birefringence of the crystal. The off-axis components of the pump polarization gets rotated by the crystal and interfere because the crystal is slightly shaped like a wedge. Because the polarization of the off-axis components is slightly altered it will pass partially through the polarizer. Rotating the $\lambda/2$-plate will minimize this effect and as a consequence one achieves the optimal polarization.

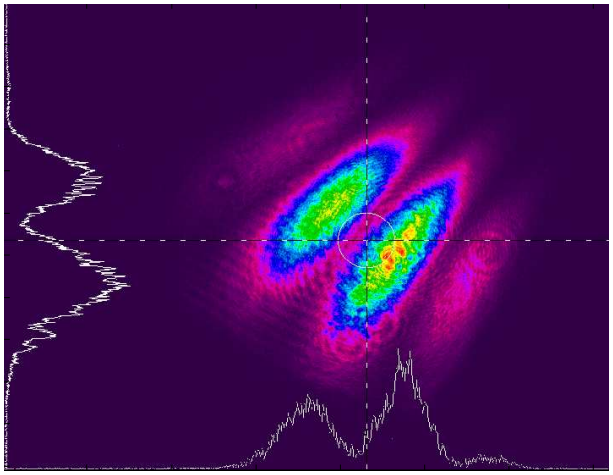

Fig. 2: Interference fringes when the pump polarization is not properly aligned to the crystal axis.

3.1.2 Finding the position of the crystals output facet

To find the output facet of the crystal and lock the position on the motion controller is straightforward. One illuminates the crystal from the back (seen from the point of view of the CCD-camera) with an extended light source. Then

find a sharp image of the output facet on the CCD by moving the crystal in the z-direction with actuator. Once a sharp image is found (see Fig. 3) the position counter on the motion controller is set to zero as a reference.

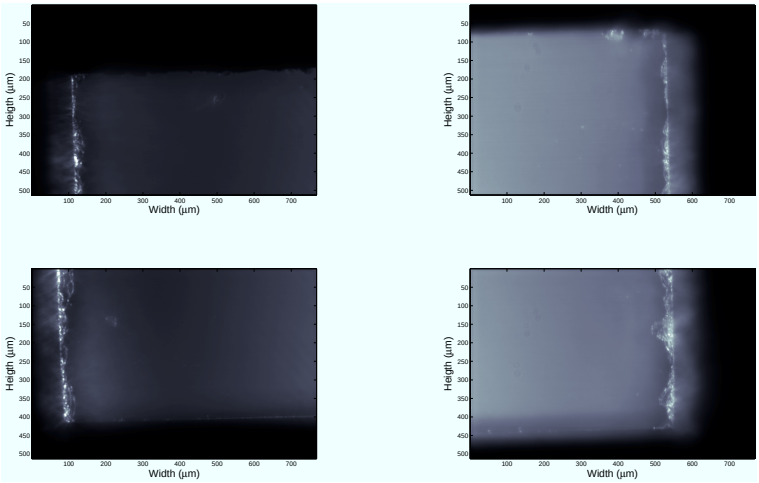

Fig. 3: The four corners of the front facet (seen from the point of view of the CCD-camera) of the crystal facing the CCD-camera, illuminated from the back of the crystal. This image shows where the image plane is with respect to the crystal and allows one to position it in the center of the crystal.

3.1.3 Aligning the beam waist with the image plane

Aligning the pump focus with the image plane involves a three step process in which we minimize the width of the observed SPDC intensity profile. The first step is to turn the dial of the pump lens so that the focus is well outside the image plane of the CCD-camera. After that the dial is turned through the image plane in incremental steps of $\approx$250 μm and a picture is taken at each step. This is done near perfect collinear phase-matching so that the intensity profile can be approximated by a Gaussian. The pictures are then imported into an array in MATLAB. Of each picture the center of the image is located by an algorithm and a cross section is made and stored into a different array. In the second step all of the cross sections are then fitted with a Gaussian and the full width at half maximum is then extracted from the fit and stored in a vector. In the third step this vector is plotted (see Figure 4) as a function of position and fitted with the following model

$$w(z) = w_0 \sqrt{1 + \left[\frac{\lambda(z-a)}{\pi w_0^2}\right]^2}, \tag{18}$$

where λ=413.1 nm and w_0 and a are fit parameters; the value of a will yield the optimal alignment setting. This way alignment is found with best possible accuracy.

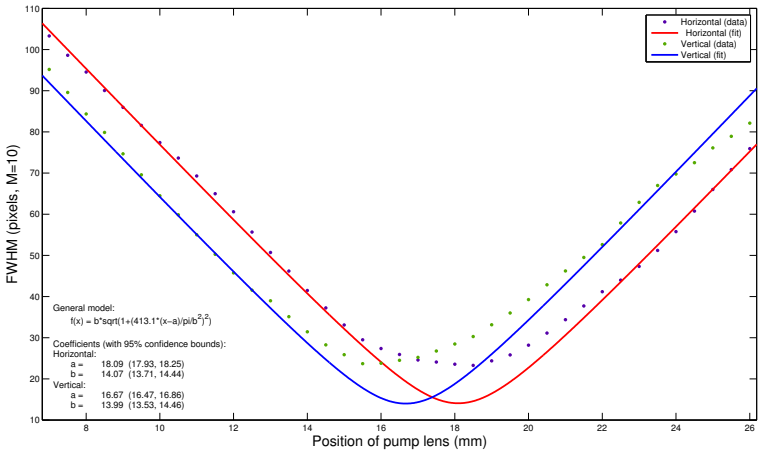

Fig. 4: In this figure the width of the SPDC intensity profile is plotted against the position of the focus waist with respect to the image plane around perfect collinear phase-matching. The shape of the intensity pattern can then be approximated with a Gaussian profile. This way we can align the image plane with the focus waist to obtain optimal resolution. The red and blue curves are for the horizontal and vertical cross sections. Notice that there is some astigmatism. This can be caused by the ellipticity of the pump.

3.2 Results and discussion

3.2.1 Temperature dependence of the total SPDC power

We measured the temperature dependence of the total SPDC power by putting a photo diode behind the PPKTP crystal. The SPDC light is then focussed into the detector by a lens. A 826/5 nm band-pass filter is placed in front of the detector to measure at frequency degeneracy. Laser power is set to 100 mW to get a good signal to noise ratio. The result of this measurement is displayed in Fig. 5. The total power of the SPDC light is proportional to the integral of the square of the phase-matching function over the illuminated area. We take the area to be infinitely large:

$$\begin{aligned} P_{SPDC} &\propto \int_A \operatorname{sinc}^2(c\rho^2+\varphi)\; dA \\ &= \int_0^{2\pi}\int_0^{\infty} \operatorname{sinc}^2(c\rho^2+\varphi)\rho\; d\rho d\vartheta \\ &= \frac{\pi}{c}\left\{\left[\frac{\pi}{2}-\operatorname{Si}(2\varphi)\right]+\frac{1}{2\varphi}\left[1-\cos(2\varphi)\right]\right\}, \end{aligned} \tag{19}$$

where $\operatorname{Si}(x)$ is the *Sine Integral* of x, defined $\int_0^x \frac{\sin(t)}{t}\; dt$. Eq. (19) has limits $\frac{\pi^2}{c}$, $\frac{1}{2}\frac{\pi^2}{c}$, 0 for $\varphi \to -\infty$, 0, ∞ respectively, so it reaches half of its maximum at phase-mismatch $\varphi \propto T - T_0 = 0$. In the fitted model we made the substitution $\varphi = \alpha(T - T_0)$. We measured T_0=60.76±0.02°C and α=4.0±0.3 K^{-1} at

λ=826 nm. This is in good agreement with previous measurements[6].

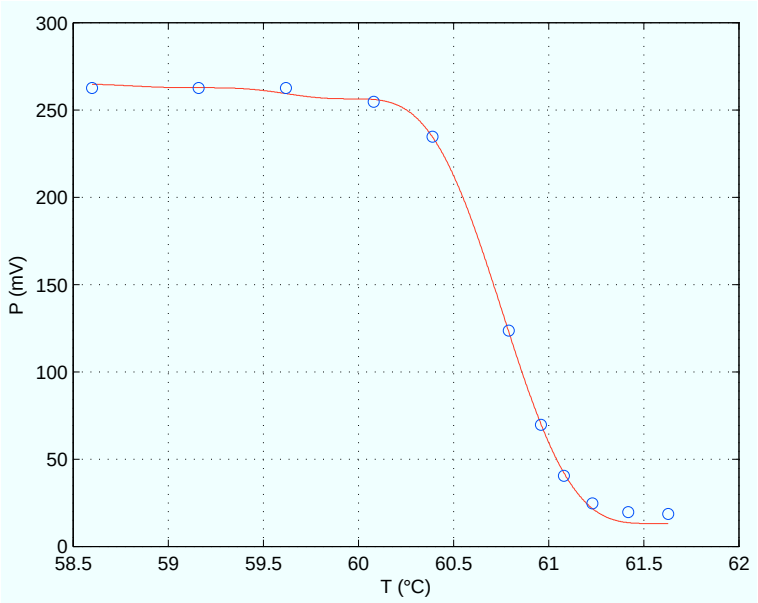

Fig. 5: SPDC power dependence on temperature. The measured data is indicated by the blue circles. The red curve is the fitted model (Eq. 19).

To determine the value of α via the ring structures we made several far-field images (see Fig. 6.) of the SPDC light at different temperatures without focussing the pump too strong ($z_p \gg L$). From each of these images a cross section is made showing the angular intensity distribution. These cross sections are then fitted to $I(\rho) = A\,\mathrm{sinc}^2\left(c\rho^2 + \varphi\right) + I_0$ (see Section 2.2.2), where A, c, φ and I_0 are fit parameters. The extracted values of φ are then plotted as a function of T and fitted again to $\varphi(T) = \alpha(T - T_0)$. The measured value is $\alpha \approx 2.71\ \mathrm{K}^{-1}$. This value is too small. The reason for this is that by the radius of the rings we can only fit the ratio $\frac{\alpha}{c}$ accurately. The individual values of α and c then follow from the width of the ring which is more difficult to determine accurately. This leads to non-unique solutions. If we use a different approach and use the theoretically calculated value of c instead, α is overestimated to be $4.7 \pm 0.1\ \mathrm{K}^{-1}$.

Measuring the value of α through measuring the total SPDC power proves to be more reliable then by successive extraction of φ at different temperatures in the far-field profile. In retrospect this is not so surprising, since the total SPDC power is a function of T only, whereas the far-field intensity is a function of ρ *and* T. Measuring the total SPDC power we need only one measurement curve to extract T_0 and α; for the far-field we need a whole bunch of cross sectional curves and still we can only get the ratio α/c accurately out of it.

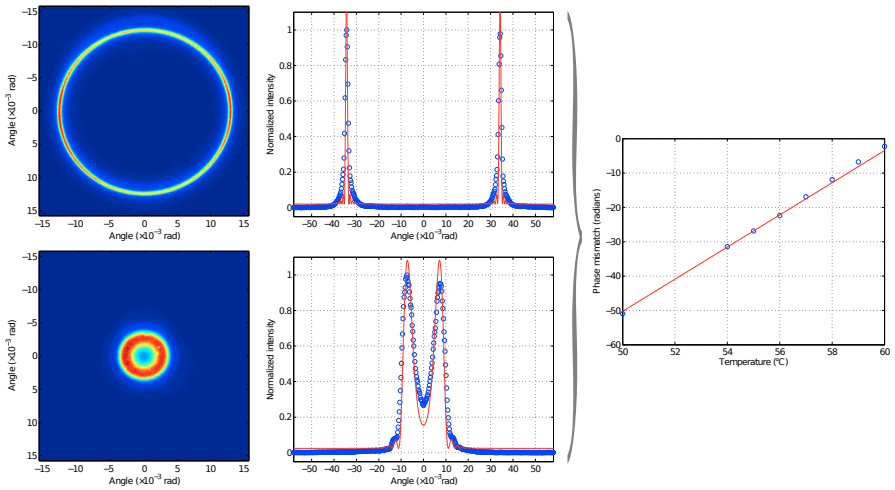

Fig. 6: The two left most pictures are false color images of the angular SPDC intensity distribution. The top one is made at T=50°C and the bottom one at T=60°C. The two middle images are horizontal cross sections along the centres of the left images. The blue circles are the data points and the red curves are fitted models with a theoretical value of c=4.33×10^{-2} mrad^{-2}. In the right most image the collinear phase-mismatch parameter φ is plotted as a function of temperature. The slope of this curve yields a value of α=4.7±0.1 K^{-1}

3.2.2 Transverse correlations of the SPDC emission

To measure the transverse profile of the down-converted light we have made pictures (see Fig. 7) at different temperatures, while keeping the position of the image plane inside the crystal constant. In Fig. 8 a representative set of cross sections is plotted, taken at different temperatures. The size of these structures is roughly 100 μm. These structures are ≈5× larger than the spot size of the pump. The shape of these structures resemble the sinc-like features of the two-photon phase-matching function covered in the theory section (Sec. 2).

3.2.3 Longitudinal correlations of the SPDC emission

If we keep the temperature constant and make pictures at different z-planes inside the crystal we are able to map the longitudinal correlations of the SPDC light. We do this by programming the actuator on the crystal translation stage to scan de position of the crystal over its full length. At each small equidistant step the program automatically captures a picture. After the program is completed a cross section is made of each picture; the cross sections are then put back-to-back to build a 3-dimensional surface that characterizes all spatial aspects of the down-converted light at a specific temperature (Fig. 9a). These spatial profiles closely resemble the ones made in a previous experiment with a coincidence setup mapping the full spatial correlations of the two-photon field. The two peaks at the facets are associated with preferred emission on account of the

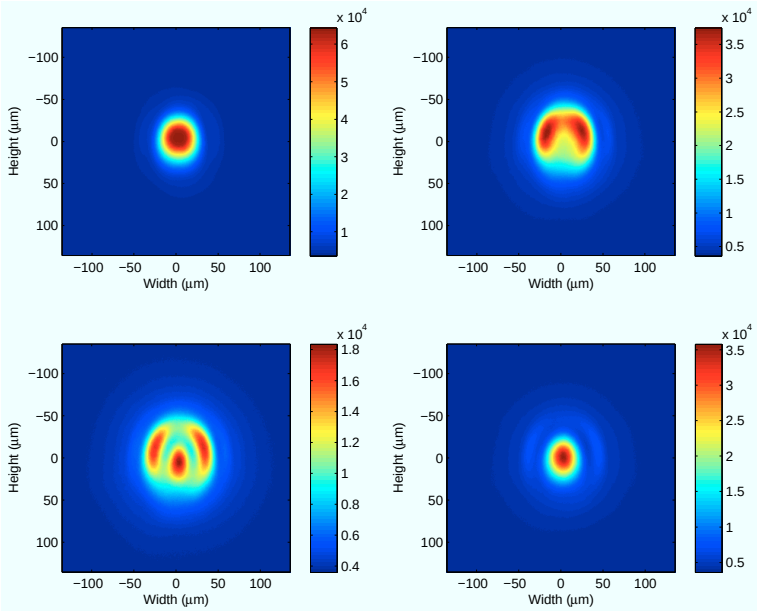

Fig. 7: Typical near-field false color images of the SPDC light. All pictures are taken under sharp imaging of the center of the crystal. The upper left image is at T=60.75°C (collinear phase-matching). The upper right image is at T=61.05°C, the lower left at T=61.20°C and the lower right at T=61.45°C.

Gouy phase shifts of the pump beam and the generated SPDC light[7].

When an on-axis (x=y=0) cross section is made (Fig. 9b) we can immediately calculate the length of the crystal by using the peak-to-peak distance and multiplying it by the refractive index n=1.7573 at λ_0=826 nm for our polarization. The thus determined physical length is 11.4±0.1 mm×1.7573= 20.0±0.2 mm, which is surprisingly close to the length of 20.08 mm specified by the manufacturer (Raicol Crystals Ltd.).

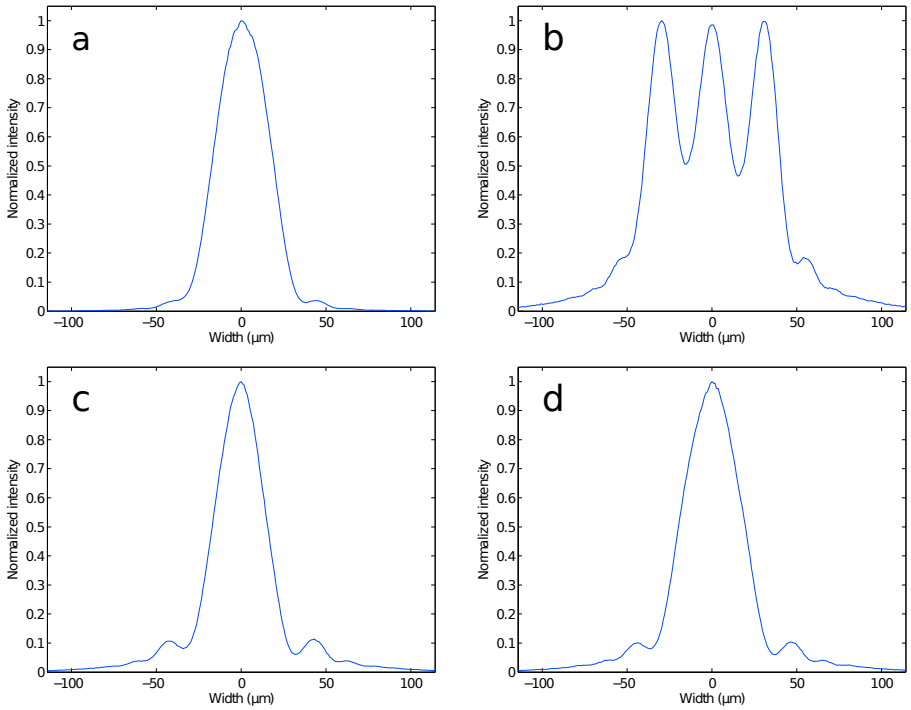

Fig. 8: Cross sections through the centres of images like those in Fig. 7. a) T=60.70°C b) T=61.20°C. c) T=61.50°C. d) T=61.60°C.

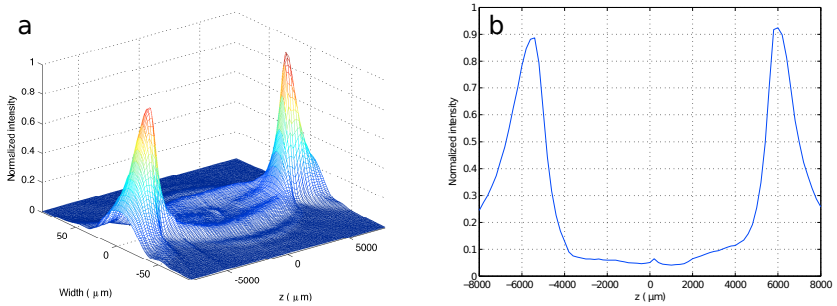

Fig. 9: a) Cross sections taken at different z-planes inside the crystal at T=62.00°C. The cross sections are put back-to-back to make a 3-dimensional image and give an impression of the full spatial profile of the SPDC process inside the crystal. b) On-axis cross section along the z-direction. The picture clearly shows the two pronounced peaks at the input and output facet of the crystal. The peak-to-peak distance is measured to be 11.4±0.1 mm. This corresponds to a physical crystal length of 20.0±0.2 mm.

4 Imaging the two-photon field

4.1 Experimental setup

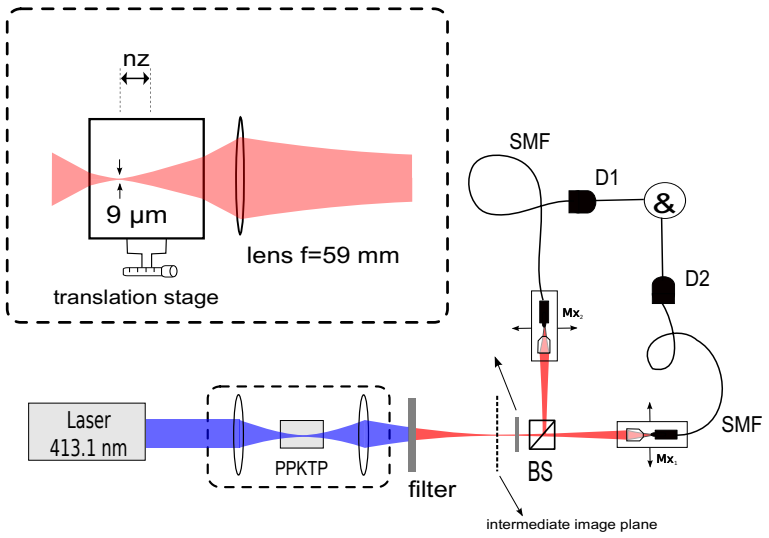

Fig. 10: Experimental setup for measuring the near-field correlations of the two-photon field. A certain plane in the crystal is imaged 10× magnified onto an intermediate plane. After that, the spatially entangled photon-pairs are separated with a beam-splitter and coupled with an objective lens into single mode fibres where the photons are detected with photon counters and coincidence electronics. The inset shows how the detection modes can be traced back with a 826 nm diode laser. The width of the detection modes is approximately 9 μm which is small enough to probe the near-field correlations and big enough to get a proper signal.

To measure the quantum correlations of the two-photon field a different kind of setup is needed. We need to split-up the SPDC emission into two identical beam paths. At the end of each path a single photon counting module (SPCM) is placed. The two detectors are connected to a coincidence gate that only registers the events that both detectors are hit by a photon at the same time. By independently scanning the detectors in the transverse plane we can build a map of probabilities which tells us at what position of the detectors it is most likely to have a simultaneous incidence.

The CCD-setup discussed in Section 3 is modified as follows. The part from the $\lambda/2$-plate up to and including the second lens can by left unmodified. The f=59 mm lens now sharply images a 10× magnified plane in the crystal on an intermediate image plane, instead of a CCD. Behind this lens we still use the GaP-filter to block out the pump. A 826/5 nm band-pass filter and a 50/50 non-polarizing beam splitter are placed behind the intermediate image plane to enforce frequency degeneracy. After the beam splitter two translation stages are placed, one at each output path, to couple each beam into a single mode fibre through an objective lens. The translation stages have three degrees of freedom:

two to adjust the relative transverse position of the fibre with respect to the objective lens, to optimize the coupling into the fibre, and one to adjust the relative longitudinal distance between the objective and the fibre, to align the detection modes with the image plane. Two extra degrees of freedom are driven by computer controlled actuators connected to a Newport Motion Controller. With these actuators we can scan the detection modes (objective and fibre as a whole) in the image plane. The fibres themselves lead the light to the single photon counting modules which are connected to coincidence electronics. The scanning of the detection modes is done by a Labview program and fully automated. A schematic of the setup is displayed in Fig. 10.

4.1.1 Beam/fibre coupling and alignment of the detection modes

The easiest way to position the objective/fibre stages is to temporary remove the GaP-filter and follow the pump beam with a white paper card through the beam splitter to the objective lenses on the translation stages. A by-eye-inspection is enough to make sure the laser light hits the input tip of the fibre. Fine adjustment can be done later. The distance from the objective lenses to the intermediate image plane is positioned roughly to get a w_d=9 μm detection waist inside the crystal, or a w_d=90 μm on the intermediate image plane. Fine adjustment is later done by changing the distance between the objective and the fibre.

It is very important that both detection modes are focused in a common z-plane to make sure that the detectors are looking at photons belonging to pairs created in the same plane. The waists of the detection modes are aligned to the image plane by connecting the other end of the fibres with a 826 nm diode laser and minimizing the beam waist in the intermediate image plane, using a chopper and a photo diode connected to an oscilloscope. The smaller the waist the steeper the slope of the signal gets. By adjusting the distance between the input tip of the fibre and the objective a minimum is found relatively easily and both detection waists are now aligned to a common plane.

4.1.2 Optimizing the detection of coincidences

Once the setup is aligned the program will detect single counts on both detectors. To fine tune and optimize for coincidences is something of an art. First of all the singles counts should not be too high. A 1000-2000 kc/s single count rate works best. Lower than that, the noise becomes a problem. At rates higher than 2000 kc/s the non-linearity of the detector, associated with their dead time of 30-50 ns, becomes noticeable. To avoid this the $\lambda/2$-plate can be turned to deliberately misalign the pump polarization with the crystal axis in order to lower the conversion efficiency. Lowering the power of the pump is not a good idea because the pump power is far less stable below a certain value. This instability will introduce extra noise to the signal and will give noisy data which can only be cleaned-up by an iterative data smoothing algorithm.

The first thing to do is maximize the single counts on one of the detectors by "beam walking". This can be done by adjusting one axis (e.g. the x-axis) with

the actuator and watch the signal rise, or drop. Slightly adjusting the relative position of the fibre and the objective lens in the same direction (x-axis) so that the count rate will drop again (effectively changing the in-coupling). Now the actuator can be adjusted again to see if the count rate will rise to higher value than before. If this is the case, a new local maximum is found and the process can be repeated to find the global maximum. If not, the dial to adjust the in-coupling needs to be turned the other way around followed by adjusting the actuator again. After this iterative process the single counts in that direction is maximized. This has to be repeated for the other direction as well and for both detectors.

After the maximum for both x- and y-directions for both detectors is found their positions on the motion controller need to be reset to zero to center the maximum and allow for scanning symmetric and anti-symmetric coordinates. After the reset a scan of the transverse plane is made. First in one direction then in the other. When the singles are plotted, a Gaussian can be fitted and the location of the maxima can be quickly read off. The remaining small offset from zero can be corrected by adjusting the actuators and resetting them to zero again.

The detectors are now accurately aligned. This has to be done every time the laser has been turned off and on because the laser will have shifted slightly. If the single counts become too high during the alignment, the $\lambda/2$-plate can be used to reduce the single counts to drop to an acceptable level. The facets of the crystal is found by scanning the actuator on the crystal stage in order to find the peaks in the singles. To align the pump focus to the image plane the pump lens needs to be adjusted as well. By watching the singles and coincidences the optimal setting can be found relatively easily.

4.2 Results and discussion

4.2.1 Transverse and longitudinal correlations

To map the full transverse correlations in one direction, a scan is made in the center of the crystal at T=61.00°C. First we make sure that the zero-position of the two detectors coincide with the center of the imaged plane. This is done by careful calibration with the method discussed in Section 4.1.2. Then one of the detectors is set to a position on the far end of one axis, say the x-axis, while keeping its y-coordinate constant at $y = 0$. The other detector is then set to the same position as detector one as its initial position. The second detector then scans the x-axis, also keeping its y-position constant. When the second detector is finished scanning the axis, the first detector is set to a new position just next to its initial one along the x-axis. The second detector again scans the entire axis, beginning at its initial position. This procedure is repeated until the first detector has covered all the points on the x-axis thereby filling a two dimensional matrix with coincidence counts, effectively determining $R_{cc}(X_1, X_2)$. The result of this scan is displayed in Figure 11. One of the diagonals correspond to the sum-coordinate part of the correlation function (Eq. 6), the narrow Gaussian profile of the pump. The other diagonal corresponds to the difference-coordinate

part; it shows the features of the phase-matching function. These diagonals are displayed in Figures 13 and 12.

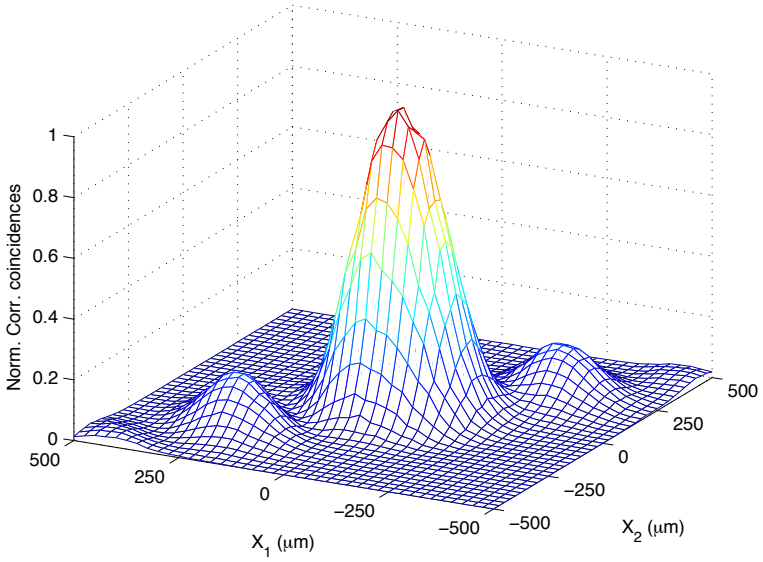

Fig. 11: The full transverse correlations in the centre of the crystal at T=61.00°C. The two diagonals correspond to the sum and difference coordinate part in Eq. 6.

To map all transverse and longitudinal correlations we scan three actuators at once, two actuators for the transverse correlations and one to scan different planes inside the crystal, keeping only the temperature constant. Only the difference scan in the transverse plane is of interest because a sum scan would only reveal the profile of the pump, which is the same everywhere because G does not depend on the z-coordinate. The scan starts at one z-plane and then scans both transverse detectors at once in opposed directions. An integration time of one second per point is used to get enough coincidence counts. After one transverse direction is scanned the program moves the crystal to another z-plane and another transverse scan is made. This will continue until the desired range is scanned. In Figure (14) the full spatial correlations are shown for T=61.39°C which corresponds to an on-axis phase mismatch of φ=1.7.

Comparing figures 8a and 12a we conclude that the spatial extent of the transverse structures in the one-photon intensity and the two-photon correlation function are approximately equal and have similar shapes, as predicted by the theory in Section 2. These are actually the only two figures that make sense to compare, because the shape of the transverse profile depends on the longitudinal position where the picture is made inside the crystal. Even for one specific temperature one can have figures like 8b,c and 12c,d at different planes inside the crystal. An exception to this plane dependence is the temperature where the phase mismatch is zero. At that temperature the transverse shape of the profile does not change very much. So the comparison is easy only at that temperature.

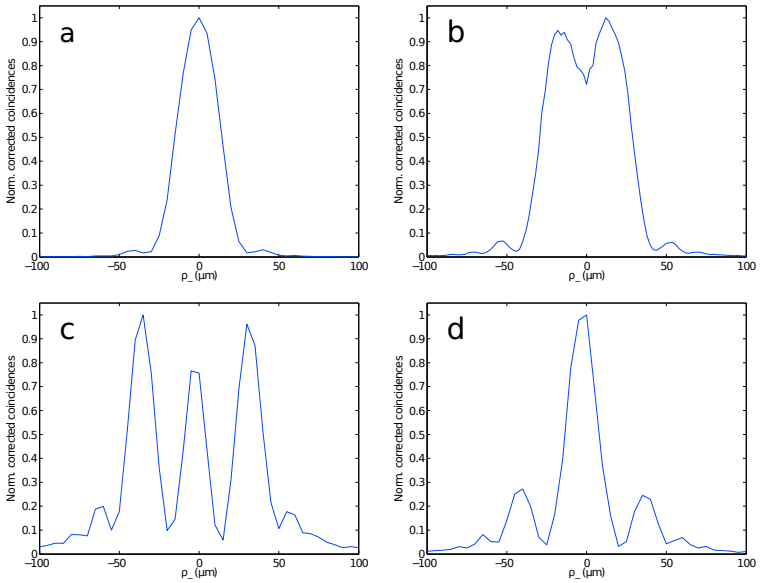

Fig. 12: Difference coordinate scan in the middle of the crystal at four different temperatures. a) T=60.70°C b) T=61.20°C. c) T=61.50°C. d) T=61.60°C.

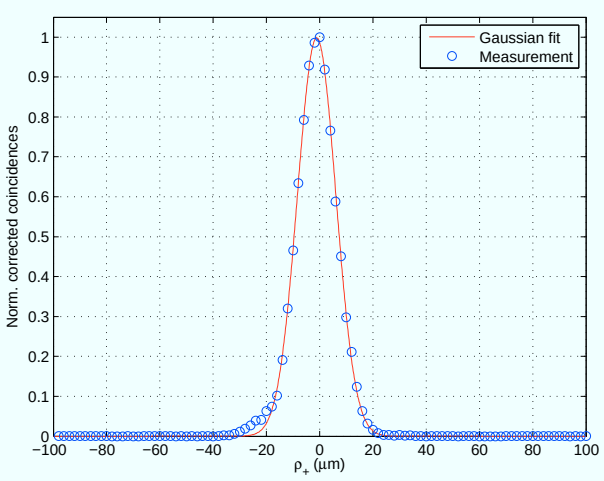

Fig. 13: A sum coordinate scan at T=61.20°C in the center of the crystal. A Gaussian is fitted to the data and its $1/e^2$ width is measured to be 10.2μm. This is approximately equal to the waist of the pump, which is w_p=11μm.

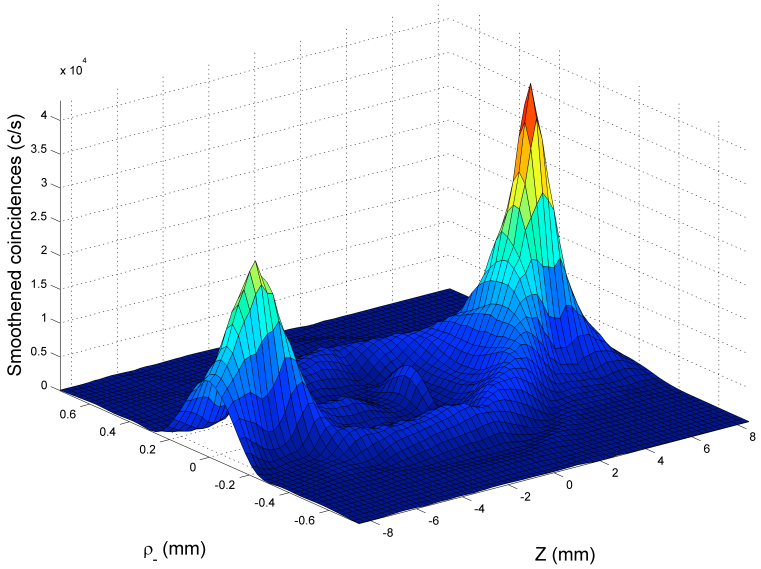

Fig. 14: A full spatial difference scan. At T=61.39°C transverse difference scans are made at several equally spaced planes inside the crystal and stacked back-to-back to obtain this image. The two peaks at the facets are very prominent. There is also a "bump" in the middle. A transverse cross section here looks very similar to a cross section from Figure 9 obtained at T=62.00°C.

4.2.2 Scanning the focus of the pump

The important differences between this two-photon experiment and the previous two-photon experiment, discussed in [1], is that we now focus the pump very strongly and use a crystal that is 4× longer. This enables us to look at the on-axis correlations while scanning the pump. In the case were $\boldsymbol{\rho}_+ = \boldsymbol{\rho}_- = \mathbf{0}$, the two-photon correlations will reduce to a Lorentzian type relation:

$$\begin{aligned} R_{cc} &\longrightarrow R_{cc}(Z_d - Z_p) \\ &\propto \frac{1}{(z_d + z_p)^2 + (Z_d - Z_p)^2} \\ &\propto I \left[\frac{\gamma^2}{(Z_d - Z_p)^2 + \gamma^2} \right], \end{aligned} \tag{20}$$

with scale parameter $\gamma \equiv z_d + z_p$ and $I \equiv \frac{1}{\gamma^2}$. The half width at half maximum of this function is fully determined by the Rayleigh range of the pump and the detection modes. Then we fix position of the detection modes at $Z_d \approx -L/2$ (the input facet) and scan the pump to determine $R_{cc}(Z_p)$.

For this measurement the manual dial on the pump-lens translation stage is replaced with a computer controlled actuator. A scan is then made of the position of the pump focus, starting a couple of millimetres in front of the imaged plane. Then in small equidistant steps measurements are done until the the focus of the pump has gone through the imaged plane ending symmetrically at the other

side. The resulting data is displayed in Figure 15 and fitted with a Lorentzian. The scan is made with the detection modes near the input facet of the crystal for an optimal coincidence rate and low noise floor. Notice the small asymmetry around Z_p=0. The data points on the left are slightly below the fitted model. This side corresponds to the part of the scan where the focus of the pump is outside of the crystal. The right side, which follows the model more closely, corresponds to the part of the scan inside the crystal.

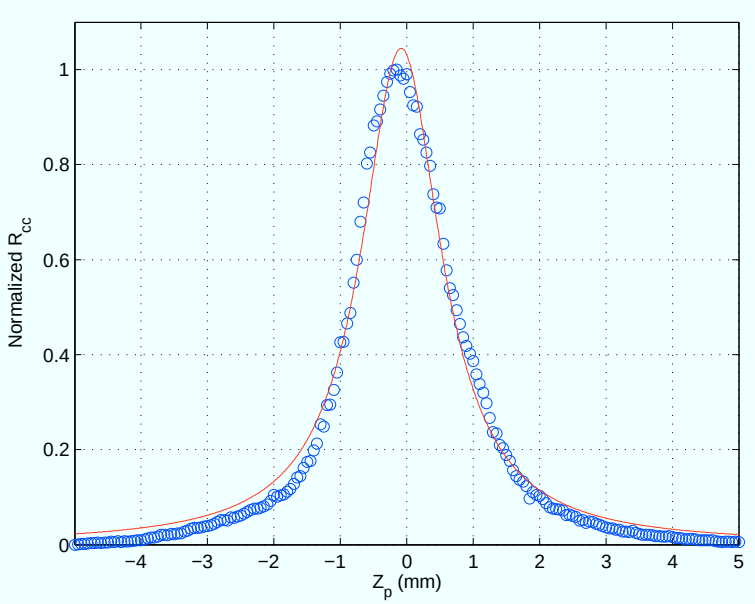

Fig. 15: The on-axis coincidences as a function of the distance between de pump focus and the detection modes at T=60.00°C. The coincidences show a Lorentzian dependence on the pump-detection mode distance. I=1.045, γ=0.732 mm. The location where R_{cc} attains its maximum value slightly deviates from zero due to the small asymmetry; Z_p =0.084 mm (Eq. 20)

5 Summary

In this report we have studied the spatial aspects of spontaneous parametric down conversion with a strongly focussed pump. We conclude that

- the two-photon spatial correlations approximately retain their specific shape under strong focussing
- it can be shown theoretically that the near-field correlations in the two-photon field can be made visible in the one-photon field by taking the partial trace over one of the photons in the two-photon field and approximating the pump field by a Dirac delta function
- these correlations can be made visible experimentally by means of a CCD-camera
- the observed structures in the one-photon intensity field closely resemble those observed in the two-photon correlation images
- the spatial correlations in the two-photon field retain their shape when the pump focus is moved away form the focus of the detection modes. Only the magnitude of coincidence count rate decreases, exhibiting a Lorentzian-type dependence.

References

[1] Di Lorenzo Pires, H. and van Exter, M. P. *Phys. Rev. A* **80**, 053820 Nov (2009).

[2] Di Lorenzo Pires, H. and van Exter, M. P. *Phys. Rev. A* **79**, 041801 Apr (2009).

[3] Saleh, B. E. A., Teich, M. C., and Sergienko, A. V. *Phys. Rev. Lett.* **94**, 223601 Jun (2005).

[4] Hong, C. K. and Mandel, L. *Phys. Rev. A* **31**, 2409–2418 Apr (1985).

[5] Monken, C. H., Ribeiro, P. H. S., and Pádua, S. *Phys. Rev. A* **57**, 3123–3126 Apr (1998).

[6] Peeters, W. H. and van Exter, M. P. *Opt. Express* **16**, 7344–7360 (2008).

[7] Kleinman, D. A., Ashkin, A., and Boyd, G. D. *Phys. Rev.* **145**, 338–379 May (1966).